

CIV AND CIII] REVERBERATION MAPPING OF THE LUMINOUS QUASAR PG 1247+267

D. TREVESE¹, M. PERNA², F. VAGNETTI³, F.G. SATURNI^{1,4}, AND M. DADINA⁵

¹Dipartimento di Fisica, Università di Roma La Sapienza, Piazzale Aldo Moro, 5, 00185 Roma, Italy

²Dipartimento di Fisica e Astronomia, Università di Bologna, Viale Berti Pichat 6/2, 40127 Bologna, Italy

³Dipartimento di Fisica, Università di Roma Tor Vergata, Via della Ricerca Scientifica 1, 00133 Roma, Italy

⁴European Southern Observatory, Karl-Schwarzschild-Strasse 2, 85748 Garching bei München, Germany

⁵INAF-IASF Bologna, Via Gobetti 101, 40129 Bologna, Italy

Draft version April 3, 2015

ABSTRACT

So far the masses of about 50 active galactic nuclei have been measured through the reverberation mapping technique (RM). Most measurements have been performed for objects of moderate luminosity and redshift, based on H β , which is also used to calibrate the scaling relation which allows single-epoch (SE) mass determination based on AGN luminosity and the width of different emission lines. The SE mass obtained from C IV(1549Å) line shows a large spread around mean values, due to complex structure and gas dynamics of the relevant emission region. Direct RM measures of C IV exist for only 6 AGNs of low luminosity and redshift, and only one luminous quasar (Kaspi et al. 2007). We have collected since 2003 photometric and spectroscopic observations of PG1247+267, the most luminous quasar ever analyzed for RM. We provide light curves for the continuum and for C IV(1549Å) and C III] (1909Å), and measures of the reverberation time lags based on the SPEAR method (Zu et al. 2011). The sizes of the line emission regions are in a ratio $R_{CIII]}/R_{CIV} \sim 2$, similar to the case of Seyfert galaxies, indicating for the first time a similar ionization stratification in a luminous quasar and low luminosity nuclei. Due to relatively small broad line region size and relatively narrow line widths, we estimate a small mass and an anomalously high Eddington ratio. We discuss the possibility that either the shape of the emission region or an amplification of the luminosity caused by gravitational lensing may be in part responsible of the result.

Keywords: Galaxies: active - quasars: general - quasars: emission lines - quasars: supermassive black holes - quasars: individual: PG 1247+267

1. INTRODUCTION

Reverberation mapping (RM) has played a crucial role in the study of the structure of active galactic nuclei (AGN). Spectroscopic monitoring in the UV/optical band permits to measure emission line flux changes, representing the "echo" of the far UV ionising continuum variations, which, in turn are closely related with the observed near UV continuum variations. The delay τ_l of the echo, i.e. of line variation with respect to continuum changes, is measured through the continuum-line cross-correlation and provides the luminosity-weighted average distance, $R = c \cdot \tau_l$ of the line-emitting region from the (point-like) continuum source, where c is the speed of light (Blandford & McKee 1982; Peterson 1993). Until 1999, 17 AGNs with $\lambda L_\lambda(5100\text{\AA}) \lesssim 1.5 \times 10^{44} \text{ erg s}^{-1}$ were studied (see Wandel et al. 1999, and refs therein) with the result of measuring the size of their broad line regions (BLR) and demonstrating a stratification of ionisation, with the higher ionisation lines responding more rapidly to continuum changes. Combining the size R , with a measure of the typical velocity ΔV of the emitting BLR clouds, assumed in Keplerian orbits, it is possible to derive a virial estimate of the black hole mass $M_{BH} = f c \tau_l \Delta V^2 / G$ of the central black hole, where G is the gravitational constant and f is a scaling factor depending on the geometry of the BLR and the specific definition adopted for ΔV (see section 4.). The extension of these results by the addition of a sample of 17 quasars (QSO) with luminosities $\lambda L_\lambda(5100\text{\AA})$ up to $\sim 6.5 \times 10^{45}$

erg s⁻¹, allowed Kaspi et al. (2000) to establish a size-luminosity scaling relation of the type $R \propto L^\gamma$, in a luminosity range covering more than four decades (Kaspi et al. 2005; Bentz et al. 2006, 2009). This relation can be used to estimate the BH mass on the basis of ΔV and L measured from single epoch (SE) spectra (Vestergaard 2002; McLure & Jarvis 2002), opening the possibility of estimating the BH mass of thousands QSOs/AGNs, analysing their luminosity function at different redshifts, and following the BH-galaxy co-evolution in cosmic time (Shen & Kelly 2012). The widths of different lines, H β , C IV, Mg II, are used depending on redshift and wavelength range of optical/IR ground based observations. However, the scaling relations for C IV and Mg II (McLure & Jarvis 2002; Vestergaard & Peterson 2006; McGill et al. 2008) are not obtained from the few direct RM measures of these lines, but are calibrated on the mass scale based on H β time lags, which represent the majority of RM measures to date. The latter are presently limited to objects with $\lambda L_\lambda(5100\text{\AA}) \lesssim 10^{46} \text{ erg s}^{-1}$ and $z < 0.3$ (Bentz et al. 2013, and refs therein). According to Netzer (2003), the largest black hole masses deduced from these extrapolations, occurring in objects with the highest luminosities, would exceed $10^{10} M_\odot$, and, if converted to host galaxy mass and luminosity through the statistical relation among the black hole mass, galaxy bulge mass and stellar velocity dispersion, would imply galactic bulge masses $M_{bulge} \gtrsim 10^{13} M_\odot$ and stellar velocity dispersions exceeding 700 km/s which have never been

observed, suggesting that either the M_{BH} - M_{bulge} correlations observed in the local universe are different at higher redshift, or the observed size-luminosity relationship in low-luminosity AGNs does not extend to very high luminosity. Vestergaard (2004) pointed out that the space density of such luminous quasars is so low that their local absence does not mean they don't exist. In any case, exploring the validity or failure of the size-luminosity scaling relation is of crucial importance not only to understand the physical conditions in the most luminous QSOs, but also because most of the AGN mass estimates are based this unconfirmed extrapolation, which could lead to uncertain or biased conclusions on the evolution of the AGN mass function in cosmic time.

To measure the BRL size and BH mass of luminous QSOs, in 2003 we started a monitoring campaign of four high luminosity ($L \gtrsim 5 \times 10^{46} \text{ erg s}^{-1}$) and intermediate redshift ($2 < z < 4$) objects with the Copernico 1.82 m telescope in Asiago (Italy) and the Cassini 1.52 m telescope in Loiano (Italy). Some results on the QSOs PG 1634+706, with $z = 1.337$ and PG 1247+267, with $z = 2.048$, showing the detectability of the emission line variations, were published in Trevese et al. (2007). A study of broad absorption line variability of the luminous quasar APM 08279+5255 (Trevese et al. 2013; Saturni et al. 2014) and preliminary results on RM for PG 1247+267 (Perna et al. 2014) were also presented.

At $z \gtrsim 2$ H β , is no longer observable in the optical band and reverberation can be observed for C III] ($\lambda 1909 \text{ \AA}$) and C IV ($\lambda 1549 \text{ \AA}$) lines. Reverberation measurements of the C IV line are available only for a handful of low luminosity ($\lambda L_{\lambda}(1350 \text{ \AA}) \lesssim 10^{44} \text{ erg s}^{-1}$) and low redshift ($z < 0.06$) AGN observed in the ultraviolet from space. In addition, Kaspi et al. (2007) presented the first results of a RM campaign started in 1999 with HET 11 m telescope (Ramsey et al. 1998) providing a first tentative mass estimate for S5 0836+071, a luminous ($\lambda L_{\lambda}(1350 \text{ \AA}) = 1.12 \pm 0.16 \times 10^{47} \text{ erg s}^{-1}$) QSO at $z = 2.172$, based on C IV RM. More recently, several studies discussed the unreliability of C IV based mass estimates, due to gas outflows strongly affecting the profile of this line (Netzer et al. 2007; Sulentic et al. 2007; Marziani & Sulentic 2012; Denney 2012). The fact that there is no consensus about the scatter and possible biases between C IV-based and H β -based BH masses (Greene et al. 2010; Assef et al. 2011; Runnoe et al. 2013) further increases the importance of RM measure of the size of the emitting region to constrain wind models and eventually lead to a consistent picture which includes BH mass, gas outflow and possibly its feedback on the host galaxy.

In this work we present the C IV, C III] and continuum light curves obtained for PG 1247+267, and we estimate the relevant time lags based on a method proposed by Zu et al. (2011). We also analyze the shape of C IV and C III] lines, and discuss the determination of the virial mass of the central BH, the corresponding value of the Eddington ratio and possible explanations of the anomalously high value found. The paper is organized as follows: in section 2 we describe observation and data reduction; in section 3 we discuss the estimate of time lags; in section 4 we discuss the mass estimates based on C IV, C III] RM; in section 5 we draw the conclusions.

Throughout the paper we adopt the cosmology $H_0=70$

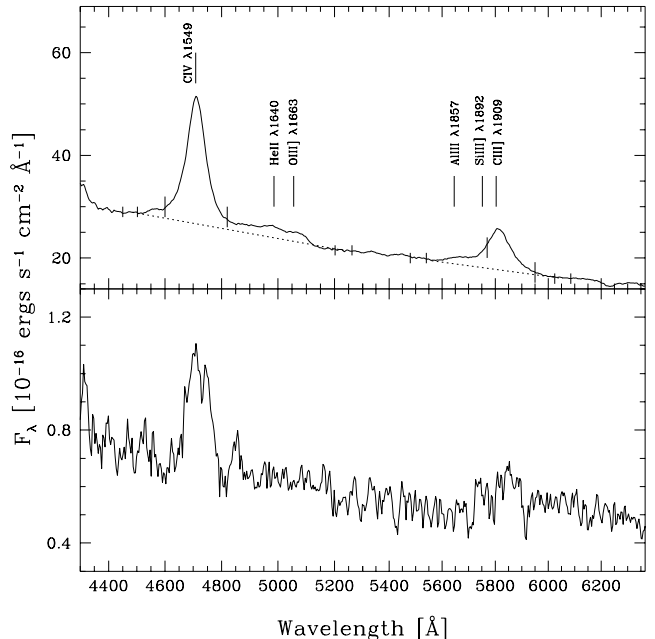


Figure 1. *Upper panel:* average spectrum of PG 1247+267 from our observations. Spectral ranges selected for the determination of the local continua (short ticks) and for the line flux (long ticks) are marked on the spectrum. Dotted lines represent the interpolated local continuum. *Lower panel:* r.m.s. spectrum as defined in Peterson et al. (1998).

km s^{-1} , Mpc^{-1} , $\Omega_m = 0.3$, and $\Omega_\Lambda = 0.7$.

2. OBSERVATIONS AND DATA REDUCTION

The majority of observations were carried out with the Faint Object Spectrograph & Camera AFOSC at the Copernico 1.82 m telescope in Asiago (Italy). We measured relative spectrophotometric variations by including a reference star in a wide ($8''.44$) slit to avoid differential flux losses caused by atmospheric refraction. The reference star is the object at $\alpha = 125011.44$, $\delta = +263332.1$ (J2000), with $V=13.824$ (Pickles & Depagne 2010). At each epoch, the observations consist of two consecutive exposures of ~ 1800 s. Typical resolution is $\sim 15 \text{ \AA}$ in the spectral range 3500-8500 \AA . Details are described in Trevese et al. (2007). The QSO and reference star uncalibrated spectra, $Q(\lambda)$ and $S(\lambda)$ respectively, are extracted by the standard IRAF¹ procedures, and the ratio $\mu^{(k)} = Q^{(k)}(\lambda)/S^{(k)}(\lambda)$ is computed for each exposure $k = 1, 2$. This quantity is independent of extinction variations and allows to reject inconsistent exposure pairs whenever $|\mu^{(2)}/\mu^{(1)} - 1|$ averaged over 500 \AA exceeds 0.04. This procedure also allows us to compute the relative flux differences, between the two exposures, which are used to estimate the statistical errors on continuum and emission line fluxes. At the i -th epoch t_i , pairs of spectra of both the QSO and the reference star were co-added to compute the ratio $\mu_i(\lambda) = Q_i(\lambda)/S_i(\lambda) = (Q^{(1)} + Q^{(2)})/(S^{(1)} + S^{(2)})$. Data separated by less than one day are combined into a single epoch data point.

¹ IRAF is distributed by the National Optical Astronomy Observatories, which are operated by the Association of Universities for Research in Astronomy, Inc., under cooperative agreement with the National Science Foundation.

The flux-calibrated spectrum of the star $F^S(\lambda)$ was obtained at a single reference epoch, and the calibrated quasar spectra were obtained for each epoch as $F_i^Q(\lambda) = \mu_i(\lambda)F^S(\lambda)$. We stress that the spectra are independent of extinction changes and detector response, thus spectral variations are also independent of telescope, detector and calibration. This allows us to include 4 spectra taken at the 1.5 m Cassini telescope of the Loiano Observatory, with the BFOSC camera. At each epoch two exposures of 2700 s were taken, with about the same resolution of AFOSC spectra.

Although the following reverberation analysis is independent of the absolute calibration, we have now revised the calibration of the spectra for possible future uses. This has been done by multiplying the calibrated spectrum of the reference star by a constant factor which makes its V magnitude, as computed from the spectrum adopting the Bessell (1990) filter profile, equal to $V=13.824$ as given by Pickles & Depagne (2010).

Figure 1 shows the flux-calibrated average spectrum and the r.m.s. spectrum of PG 1247+267. A spectral decomposition of the $\text{AlIII} + \text{Si III} + \text{CIII}$ blend indicates a SiIII/CIII flux ratio $\lesssim 0.3$. This is consistent with the corresponding ratio reported in table 2 of Bachev et al. (2004), since PG 1247+267 belongs to class B of Sulentic et al. (2002) on the basis of the FWHM of the broad component of its $\text{H}\beta$ line ($7460 \pm 220 \text{ km s}^{-1}$), as measured by McIntosh et al. (1999). The integration limits adopted further reduces by a factor ~ 2 the contribution to the computed CIII flux of SiIII , which therefore has been neglected. Similarly, the adopted continuum and integration limits should avoid the contamination of CIV flux from $\text{HeII}(1640\text{\AA})$ and $\text{OIII}(1663\text{\AA})$ emission. The lower panel of Figure 1 shows the r.m.s. spectrum. As expected, it appears more noisy than the average spectrum (cf. Denney 2012). Nonetheless, in the case of the stronger line CIV the average and r.m.s. profiles appear similar (see sect. 4).

Line fluxes are computed as $f_l = \int_{\lambda_1}^{\lambda_2} [F^{(Q)}(\lambda) - c^{int}(\lambda)] d\lambda$, where $c^{int}(\lambda)$ is the linear interpolation through the continua at shorter and longer wavelengths of each line, λ_{short} and λ_{long} , indicated in Figure 1, and the extremes of integration λ_1 and λ_2 , chosen to optimise the f_l signal to noise ratio, not necessarily coincide with λ_{short} and λ_{long} (see Trevese et al. 2007).

The uncertainties on line fluxes are estimated by computing the flux difference $\delta = |f^{(2)} - f^{(1)}|$ between the two exposures taken at the same epoch. Since the exposure time is roughly constant at all epochs, and fluxes are computed as the average between two exposures, we adopt as uncertainty on the flux $\sigma_f = \langle \delta^2 \rangle^{1/2}/2$, where the angular brackets indicate the average over the entire set of measurements. The fractional values of σ_f for continuum, CIII , CIV fluxes are 0.008, 0.021 and 0.015 respectively. Direct photometry of the field was also obtained at most epochs, to get an independent measure of the quasar luminosity changes, relative to the reference star, and to check the stability of the reference star against other objects in the field. Typically, at each epoch, R band photometry was obtained with exposures of 400 s at Asiago Observatory. Photometry is also available in R and/or V bands, from Loiano Observatory.

From the average spectrum we can estimate that the contribution of CIII line to the R and V magnitude is about 0.04 mag and 0.03 mag respectively, while the contribution of CIV is negligible in both bands. Thus we can use photometric data to measure continuum variations without altering significantly the continuum-line cross-correlation function. In doing this, we convert V to R' magnitudes assuming $R'(V) \equiv V - \langle V-R \rangle$, where the angular brackets indicate the average over those epochs when both R and V are measured. This conversion assumes that the V-R quasar color is constant. We have checked that r.m.s. color changes are of the order of 0.007 mag. Such color changes could slightly affect the amplitude of the continuum-line cross-correlation only in the case of CIII , but cannot affect significantly the estimate of the time delay. A measure of the continuum changes can be obtained also from the spectra. This has been done by fitting with a single straight line, $\log F^{cont}(\lambda) = -a \log \lambda + b$, the four data points which define the local continua (shown in figure 1). From these fits a conventional spectral continuum, at the peak wavelength of the Bessell (1990) V band, $F_C \equiv F_{\lambda}^{cont}(5300\text{\AA})$ has been defined. For the subsequent analysis (see Sect. 3), continuum flux changes have been referred to the epoch t_{ref} (MJD=53047.5) and expressed as magnitude changes $\delta m_C(t_i) = 2.5 \log[F_C(t_i)/F_C(t_{ref})]$. Similarly for line fluxes. Continuum changes obtained from broad band photometry have been reduced to the same scale defining $\delta R(t_i) = \Delta R(t_i) + \langle \delta m_C - \Delta R \rangle$, where the average is taken over all the epochs when both photometric and spectroscopic data are available.

Table 1 reports the results. Column 1: date; column 2: modified julian date MJD; column 3: Telescope; columns 4 and 5: V and R band magnitude differences with respect to the reference star; column 6: continuum changes δR obtained from broad band photometry; column 7: continuum specific flux F_C at $\lambda = 5300\text{\AA}$; columns 8 and 9: CIII and CIV line fluxes respectively.

Figure 2 reports the light curves in magnitude for continuum and emission lines.

3. MEASURING THE REVERBERATION TIME LAGS

The time lag τ_l of the emission line variation with respect to continuum changes is measured by the centroid of the continuum-emission line cross-correlation function, which can be computed through the discrete correlation function (DCF) Edelson & Krolik (1988) or by interpolating the light curves (Gaskell & Peterson 1987; White & Peterson 1994). Both methods provide consistent results for well-sampled light curves. In the case of poor sampling, both methods present technical problems (see the review by Peterson 1993). In particular the DCF becomes less sensitive to real correlations. Moreover, the estimate of a confidence interval on the measured time lag, which can be obtained by the z-transform method developed by Alexander (1997), requires to eliminate from each DCF bin all points corresponding to pairs of epochs having a measure in common. This causes the loss of part of the information contained in the data, so that the method may be not applicable if the total number of observations is too small.

We adopt a methodology, called Stochastic Process Estimation for AGN Reverberation (SPEAR), developed by Zu et al. (2011). The statistical basis of the method

Table 1
Variability measurements for PG 1247+267.

Date	MJD	Telescope ^a	ΔV	ΔR	δR	$F_{\lambda}^{cont}(5300\text{\AA})$	$f_{CIII\lambda}$	f_{CIV}
magnitudes						$[10^{-15} \text{ erg cm}^{-2} \text{ s}^{-1} \text{ \AA}^{-1}]$	$[10^{-14} \text{ erg cm}^{-2} \text{ s}^{-1}]$	
03-01-25	52665.3	L	1.660 ± 0.003	-	-0.122 ± 0.017	-	-	-
03-02-23	52694.5	L	1.665 ± 0.003	-	-0.117 ± 0.017	-	-	-
03-04-01	52733.4	L	1.696 ± 0.003	1.80 ± 0.01	-0.090 ± 0.023	-	-	-
03-05-09	52769.3	A	-	1.83 ± 0.01	-0.034 ± 0.023	2.34 ± 0.02	8.2 ± 0.2	25.6 ± 0.4
04-01-13	53017.6	A	-	1.85 ± 0.01	-0.014 ± 0.023	2.09 ± 0.02	7.0 ± 0.1	23.0 ± 0.3
04-01-14	53018.6	A	-	1.82 ± 0.01	-0.048 ± 0.023	-	-	-
04-02-12	53047.5	A	-	1.88 ± 0.01	0.013 ± 0.023	2.15 ± 0.02	7.3 ± 0.2	23.6 ± 0.4
04-03-18	53083.0	L	1.758 ± 0.003	1.83 ± 0.01	-0.035 ± 0.023	-	-	-
04-05-07	53133.9	L	1.780 ± 0.003	1.87 ± 0.01	0.004 ± 0.023	-	-	-
05-01-17	53388.6	A	-	1.86 ± 0.01	-0.006 ± 0.023	2.11 ± 0.02	7.7 ± 0.2	22.8 ± 0.3
05-03-10	53439.6	A	-	1.87 ± 0.01	0.004 ± 0.023	2.09 ± 0.02	7.6 ± 0.2	23.0 ± 0.3
05-04-26	53487.4	L	1.762 ± 0.003	1.84 ± 0.01	-0.024 ± 0.023	-	-	-
05-05-02	53493.5	L	1.775 ± 0.003	1.87 ± 0.01	0.002 ± 0.023	-	-	-
05-05-13	53503.5	A	-	-	-	2.15 ± 0.02	7.7 ± 0.2	22.9 ± 0.4
06-03-31	53826.4	L	1.771 ± 0.003	1.86 ± 0.01	-0.010 ± 0.017	-	-	-
06-04-26	53852.5	A	-	1.86 ± 0.01	-0.009 ± 0.023	2.15 ± 0.02	7.5 ± 0.2	21.4 ± 0.3
06-05-30	53886.5	A	-	1.89 ± 0.01	0.022 ± 0.023	2.10 ± 0.02	6.8 ± 0.1	22.0 ± 0.3
08-04-02	54559.4	A	-	1.89 ± 0.01	0.025 ± 0.023	2.04 ± 0.02	7.6 ± 0.2	22.5 ± 0.3
08-12-23	54823.7	A	-	1.88 ± 0.01	0.012 ± 0.023	2.18 ± 0.02	6.7 ± 0.1	23.2 ± 0.3
09-03-23	54915.7	A	-	1.87 ± 0.01	0.005 ± 0.023	2.17 ± 0.02	7.0 ± 0.1	22.7 ± 0.3
09-05-27	54979.5	A	-	1.87 ± 0.01	0.005 ± 0.023	2.16 ± 0.02	6.9 ± 0.1	23.0 ± 0.3
11-04-01	55652.5	A	-	-	-	2.00 ± 0.02	7.6 ± 0.2	25.3 ± 0.4
12-02-27	55985.5	A	-	1.96 ± 0.01	0.093 ± 0.023	2.13 ± 0.02	6.8 ± 0.1	22.5 ± 0.3
12-12-11	56272.7	L	-	1.78 ± 0.01	-0.092 ± 0.023	2.21 ± 0.02	7.2 ± 0.2	24.4 ± 0.4
13-04-13	56396.4	L	-	1.74 ± 0.01	-0.125 ± 0.023	2.37 ± 0.02	6.9 ± 0.1	23.4 ± 0.4
24-03-14	56741.6	L	-	1.80 ± 0.01	-0.073 ± 0.023	2.33 ± 0.02	6.4 ± 0.1	24.0 ± 0.4
01-04-14	56749.5	L	-	1.81 ± 0.01	-0.057 ± 0.023	2.31 ± 0.02	7.1 ± 0.1	23.3 ± 0.4

Note. — ^a A - Copernicus telescope, Asiago; L - Cassini telescope, Loiano.

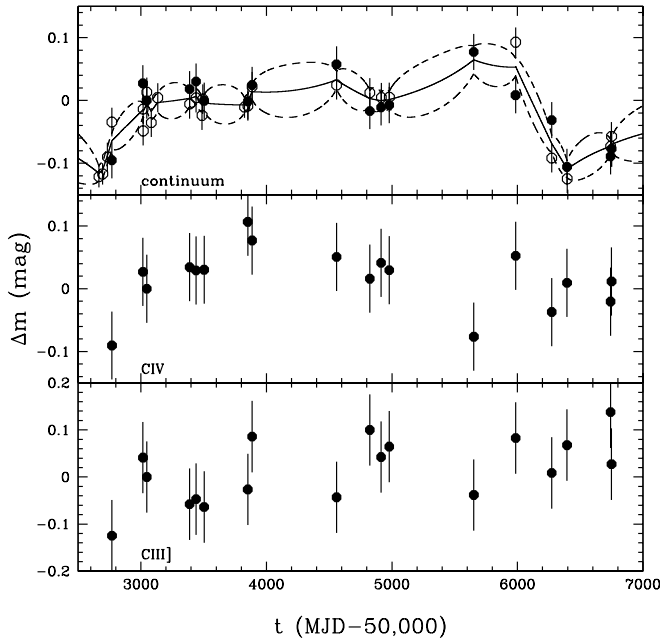


Figure 2. Magnitude changes as a function of time. *Upper panel:* continuum changes from spectrophotometry δm_C (filled circles) and from broad band photometry δR (open circles). Data interpolation (continuous line) and the relevant $1\text{-}\sigma$ uncertainty (dashed lines) according to the method of Zu et al. (2011). *Middle panel:* CIV(1549Å) line. *Bottom panel:* CIII(1909Å) line.

was introduced by Press et al. (1992) and Rybicki & Press (1992). A subsequent modification and application to RM of NGC 5548 is discussed in Rybicki & Kleyana (1994). For a detailed description of the SPEAR we refer to the paper of Zu et al. (2011). An upgraded version called JAVELIN, which allows photometric RM, is discussed in Zu et al. (2013, b). Here we recall a few important points which motivate our choice to adopt this method to measure reverberation time lags in our case. First of all, it makes use of interpolation, which is essential for us, given the small number of data points. But, while a simple linear interpolation is based on two nearby points, here the entire dataset contributes to each interpolated point, through weights which are statistically determined from the correlation functions of the data. Moreover, statistical uncertainties are assigned to each interpolated value. The uncertainties tend to the measurement errors in correspondence with the data points, and become larger and larger when the distance from the neighbor data points increases (see Figure 2). The main assumption of the method is that the emission-line flux variations $l(t)$ are scaled, smoothed, and time-shifted versions of the continuum variations $c(t)$, obtained through a transfer function $\Psi(t)$:

$$l(t) = \int dt' \Psi(t') c(t - t'), \quad (1)$$

In our analysis, we assume for $\Psi(t)$ the simple form

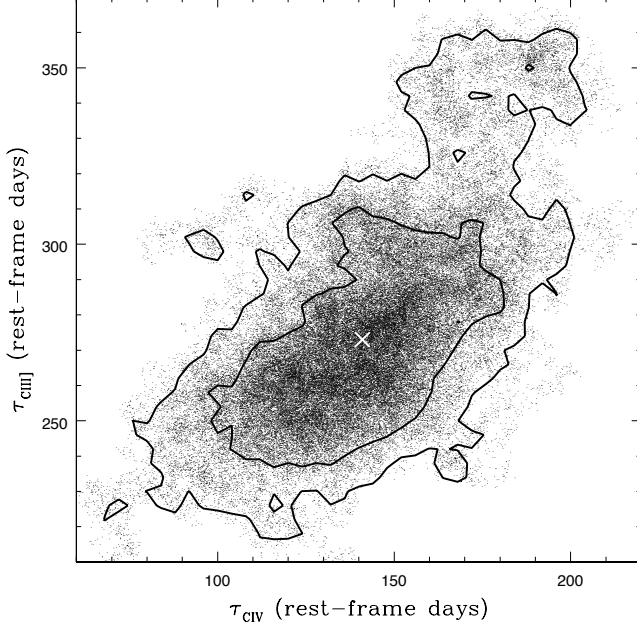


Figure 3. The distribution of points generated by 10^5 MCMC iterations in the $(\tau_{CIV}, \tau_{CIII])$ plane. Contours correspond to 68% and 95% confidence levels. The white cross indicates the median values of the marginal distributions of the two parameters.

adopted by Zu et al. (2011):

$$\Psi(t) = A/\Delta, \quad |t - \tau_l| \leq \Delta; \quad \Psi(t) = 0 \quad \text{elsewhere}, \quad (2)$$

where A , τ_l and Δ represent the attenuation, the line-continuum lag and the temporal width respectively. A maximum likelihood code determines the attenuation, smoothing and time lag parameters. The resulting emission line delay τ_l does not depend strongly on the form assumed for $\Psi(t)$ (Rybicki & Kleya 1994). The correlation functions of the data are represented by parametric models whose parameters are also determined by likelihood maximisation. This allows adding information deduced from existing data on the statistical properties of QSO light curves. In fact, it has been shown that a damped random walk (DRW) process is a good representation of QSO variability (Kelly et al. 2009; Kozłowski et al. 2010; MacLeod et al. 2010; Zu et al. 2013). The DRW auto-correlation function of the continuum changes $c(t)$ has the form:

$$\langle c(t)c(t + \tau_l) \rangle = \sigma^2 \exp(-|\tau_l|/\tau_d), \quad (3)$$

where τ_l is a time lag, τ_d is the damping time scale, σ is the variability amplitude, and angular brackets indicate the ensemble average. Another important feature of the SPEAR method is that the light curves of more lines can be included in the same fitting procedure. This provides more stringent constraints which allows better choice among the local likelihood maxima in the space of parameters.

A single fitting procedure determines the eight parameters: σ and τ_d for the continuum, the time lags τ_{CIV} , $\tau_{CIII]}$, the amplitudes A_{CIV} , $A_{CIII]}$ and smoothing parameters Δ_{CIV} , $\Delta_{CIII]}$, for the two lines respectively. SPEAR adopts a Bayesian method to determine the confidence interval in the parameters space. Once the values of the parameters which maximize the likelihood are

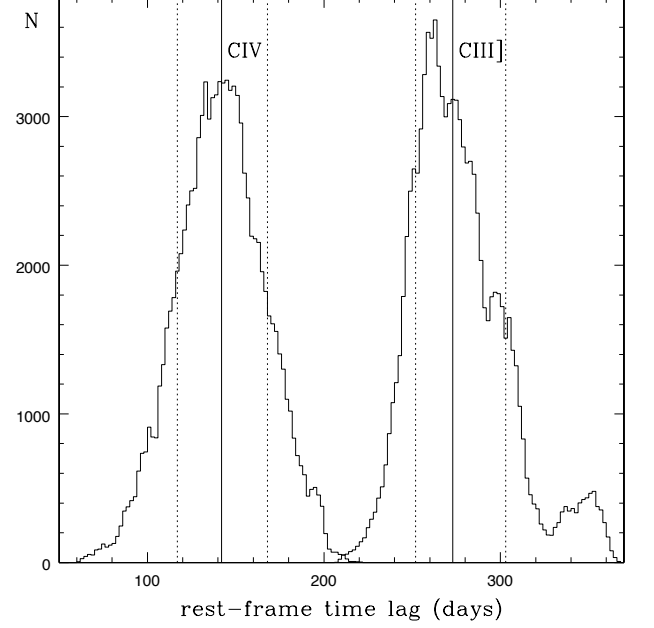


Figure 4. Posterior distributions of the rest-frame time lags τ_{CIV} and $\tau_{CIII]}$ produced by the SPEAR method with 10^5 MCMC iterations. Continuum vertical lines indicate the median values and the dashed lines indicate the 68% confidence intervals.

determined, random increments obtained from *prior* statistical distributions are applied to all parameters and the likelihood is re-evaluated. Following a Markov Chain Monte Carlo (MCMC) method (see Press et al. 2007, and refs therein), the process is iterated and a *posterior* distribution of acceptable parameters is produced. Figure 3 shows the distribution of points in the $(\tau_{CIV}, \tau_{CIII])$ plane after 10^5 MCMC iterations, and the corresponding 68% and 95% confidence regions. Figure 4 shows the relevant posterior distributions obtained separately for τ_{CIV} and $\tau_{CIII]}$. From these we take as fiducial estimate of the fitting parameters their median values, with the uncertainties defined by the 68% confidence intervals: $\tau_{CIV} = 142 \pm_{25}^{26}$ days, $\tau_{CIII] = 273 \pm_{21}^{30}$ days in the QSO rest-frame.

With respect to our preliminary results (Perna et al. 2014), the present analysis differs because: i) we fit simultaneously both CIV and CIII] light curves ii) the continuum light curve includes the available V and R band photometry, together with the continuum variations measured from the spectra, and iii) we have included photometric and spectroscopic data of three most recent epochs. Considering the small number of points and the uneven sampling, with two main gaps for MJD (53900,54500) and MJD (55000,55600), it is worth wondering whether the likelihood maxima are real or are determined by the sampling pattern. To this end, we performed a Monte Carlo simulation, generating $N = 1000$ mock, uncorrelated, continuum and emission line light curves, assuming the same set of sampling epochs, r.m.s. variability amplitude, and measurement uncertainties. We applied the SPEAR procedure to the k -th set of light curves and, once σ and τ_d were fitted, we produced a likelihood “image” $\mathcal{L}_k(\tau_l, \Delta_l)$ as a function of the lag τ_l and the smoothing parameter Δ_l , ($l = CIV, CIII]$). Then we analyzed the sum $\mathcal{L} \equiv \sum_{k=1}^N \mathcal{L}_k$, which must show local

maxima in correspondence of the points (τ_l, Δ_l) where maxima occur more frequently in the simulations, thus indicating the effect of the fixed sampling pattern. The result shows that local maxima do exist but, with respect to the case of real data: i) they are confined to much lower values of Δ_{CIV} and Δ_{CIII} , ii) they are less pronounced and, most important, iii) they are not located in the same position of the $(\tau_{CIV}-\tau_{CIII})$ plane where they occur in the case of real data.

We can conclude that it is very unlikely that the local maxima related with the sampling pattern may produce the maxima obtained in the case of the measured light curves. Thus we assume this result as first evidence that the values of τ_{CIV} and τ_{CIII} for PG 1247+267 are due to real echo lags.

We can compare them with the few corresponding RM results available in the literature. Measures of both CIV and CIII time lags from RM exist for 3 Seyfert nuclei: NGC 5548 (Peterson & Wandel 1999), NGC 3783 (Onken & Peterson 2002), NGC 4151 (Metzroth et al. 2006, and refs therein), all less luminous than $\lambda L_\lambda(1350\text{\AA}) \approx 4 \times 10^{43} \text{ erg s}^{-1}$. On average, the ratio of the time lags of these two lines is $\tau_{CIII}/\tau_{CIV} \approx 2$. While there is no reason to expect that a QSO, 10^4 times more luminous, should show approximately the same ratio, it is interesting to note that in the case of PG 1247+267 we obtain $\tau_{CIV}/\tau_{CIII} \sim 2$, i.e. the typical distance from the continuum source of the emission region of the semi-forbidden CIII line is about twice the distance of the CIV emission region. The situation is summarized in Figure 5, where we report also the relevant time lags for the QSO 2237+0305, as deduced from Sluse et al. (2011), who estimate the size of the CIV and CIII emission regions on the basis of microlensing. The corresponding point looks roughly consistent with the general trend, despite the relevant sizes are of the order of 100 times larger than those of Seyfert galaxies. A straight line fit to the data points in Figure 5, $\log \tau_{CIII} = a \log \tau_{CIV} + b$ gives $a = 0.83 \pm 0.21$ and $b = 0.43 \pm 0.19$. A fit with fixed unitary slope gives $\tau_{CIII}/\tau_{CIV} = 1.8 \pm 0.5$. The very existence of this relation can be taken as a second suggestion that we are probably measuring real reverberation time lags. This result would mean that the ionization stratification in Seyfert nuclei and luminous quasars is similar.

Figure 6 shows the relation between the emission radii $R_{CIV} = c\tau_{CIV}$ and the luminosity $\lambda L_\lambda(1350\text{\AA})$ for all the objects studied so far. For their second brightest object S5 0836+071, Kaspi et al. (2007) give $\lambda L_\lambda(1350\text{\AA}) = 1.12 \pm 0.16 \times 10^{47} \text{ erg s}^{-1}$ and a tentative value of the CIV emission line delay $\tau_{CIV} = 188 \pm_{37}^{27}$ days in the quasar rest frame and discuss the slope of the $\tau_{CIV} - \lambda L_\lambda$ relation obtained by different fitting procedures. The fit, shown in Figure 6, they obtain with the FITEXY algorithm (Press et al. 1992), corresponds to a slope $\gamma = 0.52 \pm 0.04$.

PG 1247+267 is the brightest QSO ever analyzed for reverberation and has $\lambda L_\lambda(1350\text{\AA}) = 3.92 \pm 0.02 \times 10^{47} \text{ erg s}^{-1}$, deduced from Shen et al. (2011), thus it is 3.5 times more luminous than S5 0836+071. Compared with the extrapolation of the lag-luminosity relation in Figure 6, PG 1247+267 should show a reverberation lag of about 400 days, i.e. ~ 3 times larger than observed. If con-

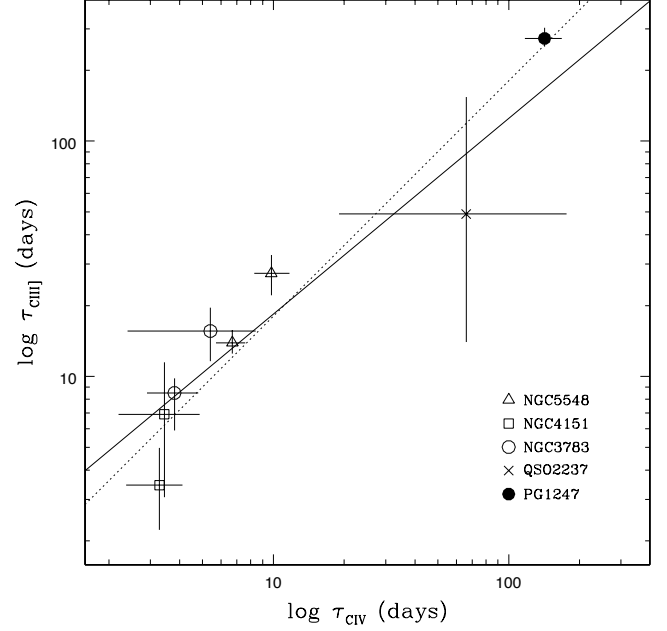


Figure 5. Reverberation time lags τ_{CIII} versus τ_{CIV} for NGC 5548, NGC 3783, NGC 4151, PG 1247+267 (our estimate). The emission region sizes (Sluse et al. 2011), converted to time lags, are also reported for the quasar QSO 2237+0305. Straight lines represent linear fits with errors on both variables: continuous line with two free parameters, dotted line with fixed unitary slope.

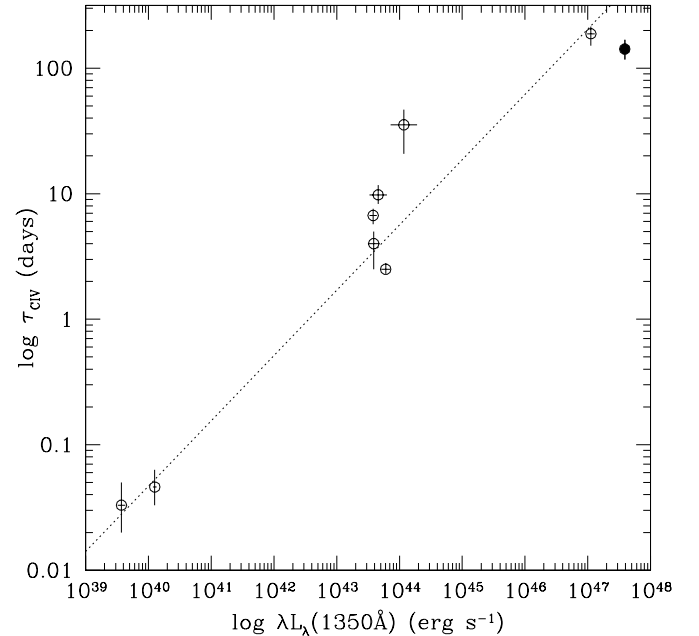


Figure 6. Size-luminosity relation obtained from CIV emission line and UV continuum. *Open circles*: data from Peterson et al. (2005, 2006) plus the values for S5 0836+71 from Kaspi et al. (2007); *filled circle*: our result for PG 1247+267. The dotted line represents the linear fit obtained by Kaspi et al. (2007) with the FITEXY method (Press et al. 1992).

firmed, this would imply a decrease of about 10% of the slope γ of the $\tau_{CIV} - \lambda L_\lambda$ relation, whose significance is marginal, however, due to the relatively large dispersion of the still small number of points in the lag-luminosity diagram for CIV. In the case of S5 0836+71, Kaspi et al. (2007) obtain $\tau_{CIII}]$ consistent with zero. A possible explanation may be that they do not use an interpolation of the light curves, which becomes necessary when the total number of points is small.

4. ESTIMATING THE VIRIAL MASS

From the emission radii $R_{CIV} = c\tau_{CIV}$ and $R_{CIII]} = c\tau_{CIII]}$, we can try and measure the BH mass through the virial relation. Unfortunately, the use of CIV emission line for mass estimation appears problematic (Netzer et al. 2007), since the profile of this line reveals the contribution of different components, whose relative weight vary so much from object to object, that the shape of this line turns out to be a good indicator of different AGN types (Sulentic et al. 2007). In principle the velocity ΔV appearing in the virial relation $M_{BH} = fR\Delta V^2/G$ could be identified with the FWHM of the emission line, or with the r.m.s. velocity dispersion along the line of sight σ_l (Peterson et al. 2004).

Under the assumption of isotropic velocity field, the kinetic energy is $K = 3/2 M \sigma_l^2$, but the numerical factor may differ from 3/2 depending on anisotropies, possibly related to the shape of the broad line clouds system. As a consequence, the numerical factor can be different for different emission lines, even in the same AGN. In the case of a Gaussian line profile, $FWHM/\sigma_l = 2.35$, but may be different for different profiles. All the numerical factors are absorbed in the factor f of the virial relation and contribute to the uncertainty of mass determination, both in the case of RM and SE measurements. In RM experiments, where several spectra taken at different times are available, it is possible to compute the r.m.s. spectrum (Peterson et al. 1998).

The non-variable parts of the spectrum, or those which vary on time-scales much longer than the experiment, do not contribute to the r.m.s. spectrum. The r.m.s. spectrum of PG 1247+267 is shown in the lower panel of Figure 1. The uncertainty on σ_l can be computed by applying a bootstrap procedure described in Peterson et al. (2004). The reason to use the r.m.s. instead of the average spectra is to avoid: i) the underestimates of ΔV caused by narrow emission line component, and ii) the effect of non virial outflows, which are expected to vary on time scales longer than reverberation time lags (see Denney 2012).

Our results are summarized in Table 2, where the reverberation time lags for both CIV and CIII] are reported, together with the relevant FWHM and σ_l , computed from mean and r.m.s. spectra. The virial products $\tau_{CIV}\Delta V_{CIV}^2$ and $\tau_{CIII]}\Delta V_{CIII]}^2$ appear consistent with the same black hole mass. We assume this fact as a third evidence that we are measuring real reverberation lags.

The numerical factor f in the virial relation can be determined empirically, by calibrating the RM masses through the $M_{BH}-\sigma_*$ relation (Ferrarese & Merritt 2000), as done for H β RM by Onken et al. (2004) who finds $f=5.5$. From the calibrated H β RM masses, Vestergaard & Peterson (2006) computed statistical scaling relations

permitting SE mass determinations on the basis of the luminosity $L_\lambda(5100\text{\AA})$ and H β line width. Scaling relations for SE mass determination based on $L_\lambda(1350\text{\AA})$ and CIV line widths, normalized to H β masses, are also provided. However, as mentioned above, the CIV line shape varies from object to object, and this causes a large spread in the measured masses around the scaling relation. A more accurate relation can be obtained by analysing the line shape parameter $S = FWHM/\sigma_l$, as computed both from the average spectrum and from the r.m.s. spectrum $\sigma(\lambda)$: S_{mean} and S_{rms} respectively. Denney (2012) pointed out that, while the ratio S_{mean}/S_{rms} is of order one for the H β line, it is different for different values of S_{mean} in the case of CIV (see her Figure 2). This is interpreted in terms of outflowing, non reverberating component not contributing to the r.m.s. spectrum. A correction, dependent on S_{mean} , is proposed to reduce the masses derived from CIV to those derived from H β (Eq.1 in Denney (2012)): $\log M_{CIV}^{corr} = \log M_{CIV}^{orig} + 0.219 - 1.63 \log(FWHM_{CIV}/\sigma_{CIV})$.

In the case of PG 1247+267, $S_{mean} = 1.85$ and the value $S_{rms}/S_{mean} = 2.2/1.85 = 1.18$ is close to one, meaning that the use of the r.m.s. spectrum does not change much the value of S , namely the effect of a non reverberating component, though present, is small. This quantifies the similarity of CIV emission line in the average and r.m.s. spectra, already noticed in Figure 1. It is interesting to note that S5 0836+071 has $S_{mean} = 1.94$ (instead of 1.85), indicating that the shapes of the CIV line of the two objects are similar. This suggests that the relevant virial factors f too are similar, so that the ratio of the masses is approximately the ratio of the virial products $\tau_l\Delta V^2$, whatever the definition of ΔV .

For the luminous quasar S5 0836+071, with $\lambda L_\lambda(1350\text{\AA}) = 1.12 \pm 0.16 \times 10^{47} \text{ erg s}^{-1}$, Kaspi et al. (2007) obtained $\tau_{CIV} = 188 \pm 27$ days in the rest-frame. They define ΔV as the $FWHM_{mean}$ and, using $f = 3/4$ in Eq.2 of Kaspi et al. (2000), they obtain a mass $M_{BH} \sim 2.6 \times 10^9 M_\odot$, which corresponds to a virial product $c\tau_{CIV}\Delta V_{CIV}^2 \sim 3.5 \times 10^9 M_\odot$. Adopting the same definition of ΔV , we obtain for PG 1247+267 $M_{BH} \sim 6.7 \times 10^8 M_\odot$, i.e. about 5 times smaller, in spite of its higher luminosity.

Using as definition of ΔV the value of σ_l obtained from the r.m.s spectra, (Onken et al. 2004) obtained an average virial factor $f = 5.5$. More recent estimates (see Pancoast et al. 2013, and refs. therein) provide different values, but we adopt conventionally the more commonly used $f = 5.5$ for the subsequent comparison with the literature. Based on this calibration, and using σ_l obtained from the r.m.s spectrum (see Table 2) we obtain $M_{BH} \sim 6.7 \times 10^8 M_\odot$.

We stress that, being the distribution of the ΔV^2 and τ_l asymmetric, some care is needed in deriving the fiducial mass values and the relevant confidence intervals. For this purpose, we computed a probability distribution of the virial product, as a function of ΔV^2 and τ_l , by multiplying the posterior distribution of τ_l (see Figure 4) and the statistical distribution of ΔV^2 obtained by the bootstrap method. From this we derived a posterior distribution of the black hole mass. In addition to the modal mass value M_{BH}^{mode} , we report in Table 3 the value computed as the centroid of the posterior distribution,

Table 2
Reverberation results for PG 1247+267

Emission line	τ_l ^a	FWHM _{mean}	$\sigma_{l,mean}$	FWHM _{rms}	$\sigma_{l,rms}$
	days	km s ⁻¹			
CIV λ 1549	142 $^{+26}_{-25}$	4939 \pm 117	2673 \pm 20	4568 \pm 1338	2104 \pm 540
CIII] λ 1909	273 $^{+30}_{-21}$	5224 \pm 63	2365 \pm 15	4752 \pm 1156	1899 \pm 713

Note. — ^a In the rest-frame

together with the asymmetric errors at 68% confidence level. Hereinafter we will use as our best estimate of the virial mass $M_{BH}^{cent} = 8.3_{-2.7}^{+3.4} \times 10^8 M_\odot$. The corresponding mass values obtained from C III] are also reported in Table 3.

We can compare our result with the summary of BH masses, known from RM, versus $\lambda L_\lambda(1350\text{\AA})$, shown in Figure 5 of Chelouche et al. (2012). From this comparison it appears that the new point, we are adding at the highest luminosity, corresponds to a mass which is roughly a factor 20 smaller with respect to the extrapolation of the general trend, which would predict a mass of the order of $2 \times 10^{10} M_\odot$. The scatter of points around the $M_{BH}-\lambda L_\lambda(1350\text{\AA})$ relation is partly intrinsic, due to the fact that different AGNs may be emitting at different Eddington ratios, and partly caused by the uncertainty on the f factor appropriate for individual objects. Thus a deviation from the average scaling relation of a factor ~ 20 is not surprising. However it deserves further discussion.

5. DISCUSSION AND SUMMARY

The number of spectral observations is still small and requires caution in deriving any conclusion. However, three independent circumstances suggest that we are probably measuring real reverberation time lags: i) despite it is reasonable to expect that the likelihood maxima might be determined by the uneven temporal sampling, Montecarlo simulations with mock random light curves, and the same sampling pattern, do not produce likelihood maxima in the same region of the parameters space; ii) the measured CIV and C III] reverberation time lag appears consistent with the $\tau_{CIV}-\tau_{CIII]}$ relation derived from the data available in the literature; iii) the virial products for CIV and C III] lines appear consistent with the same black hole mass.

Thus, assuming that the measured $\tau_{CIII]}$ and τ_{CIV} are real, we can derive some tentative conclusions.

The fact that the approximate relation $\tau_{CIII]} \sim 2\tau_{CIV}$ (see Figure 5) extends from objects with luminosity $\lambda L_\lambda(1350\text{\AA})$ from $\approx 4 \times 10^{39}$ to $\approx 4 \times 10^{47} \text{erg s}^{-1}$, if confirmed, would be a first direct evidence that the ionization stratification in luminous QSOs is similar to that found in Seyfert galaxies.

The relatively small τ_{CIV} , about 0.3 of the value ex-

pected from the extrapolation of the $\tau_l - L$ relation, tends to produce a small virial mass. The problem is made more severe by the small value of the line widths, roughly 2/3 of that of S5 0836+071 which is 3.5 times less luminous. This appears clearly when we compute the Eddington ratio L_{bol}/L_{Edd} , which contains a further uncertainty deriving from the estimate of the bolometric correction. Kaspi et al. (2007) adopt the bolometric correction of Marconi et al. (2004) (Eq.21) which refers to the luminosity $\nu_B L_{\nu B}$. For PG 1247+267 we obtain $\nu_B L_{\nu B} = 2.0 \times 10^{47} \text{erg s}^{-1}$, interpolating between the values of $\lambda L_\lambda(2500\text{\AA})$ and $\lambda L_\lambda(5100\text{\AA})$ provided by Krawczyk et al. (2013). The resulting correction is $L_{bol}/\nu_B L_{\nu B} = 5.28$, leading to $L_{bol} = 1.06 \times 10^{48} \text{erg s}^{-1}$ and $L_{bol}/L_{Edd} = 9.8$ (after a small correction for the different cosmology we adopt). A similar result, $L_{bol}/L_{Edd} \sim 10.4$ is found adopting the bolometric correction $L(1\mu - 2keV)/\nu L_\nu(2500\text{\AA}) = 3.5$ with $\log \nu L_\nu(2500\text{\AA}) = 47.50$ from Krawczyk et al. (2013).

We stress that this large Eddington ratio is due only in part to the small size of the BLR. In fact, even the SE mass estimate, which is independent of reverberation lag, produces for PG 1247+267 an Eddington ratio in the range 1.2 - 3, depending on the use of the line shape correction (Denney 2012) and the different choices of bolometric correction.

As discussed in the previous section, a possible origin of a too small line width may be the presence of a narrow emission line component, or the contribution of a possibly non variable and non virial wind component. This suggested to use, as we did, the r.m.s. spectrum. Besides this, orbits of BLR clouds are unlikely to be oriented randomly, as suggested by various evidences reviewed by Gaskell C. M. (2009), and sources viewed at a low inclination angle (nearly face-on) show a small FWHM, leading to a systematic underestimation of the black hole mass by a factor up to ~ 10 (Marziani & Sulentic 2012).

For 5 Seyfert nuclei, Pancoast et al. (2013) compute line profile models, which depend on the opening angle of the cloud distribution, for different values of the inclination angle with respect to the axis of the accretion disk. The relevant virial factor f , to be applied when using σ_l from r.m.s. spectra, can be as high as 50 for an inclination angle of 8 degrees. Thus, a plausible high value of the virial factor f could easily bring the Eddington ratio towards more common values, without, however, explaining the relatively small reverberation time lag.

The effects of orientation on the characteristics of the CIV line have been investigated by Runnoe et al. (2014). By comparison with their Figure 3, the small amplitude relatively to Si IV and narrow line width found in the spectrum of PG 1247+267 suggest, in fact, a small inclination angle, supporting a high f value. A more quan-

Table 3
Mass estimates for PG 1247+267

Emission line	M_{BH}^{mode}	M_{BH}^{cent}
	$10^8 M_\odot$	
CIV λ 1549	6.7 $^{+5.0}_{-1.1}$	8.3 $^{+3.4}_{-2.7}$
CIII] λ 1909	10.5 $^{+17.2}_{-9.1}$	9.9 $^{+17.8}_{-8.5}$

titative evidence would require, however, a dynamical modeling of the type presented by Pancoast et al. (2013), and a comparison with velocity resolved RM, not feasible with our present data.

A different, and apparently trivial, explanation of the high Eddington ratio can be an overestimate of the luminosity caused by gravitational lensing. Allowing for magnification would, at the same time, justify the apparently small BLR size. Moreover, we suggest to take into account two other concurrent clues. The first concerns the negative correlation between the $\alpha_{ox} = 0.384 \log L_\nu(2keV)/L_\nu(2500\text{\AA})$ and $L_\nu(2500\text{\AA})$ found in statistical samples of QSOs/AGNs. With respect to this relation PG 1247+267, with $\alpha_{ox} = -1.69$ and $L_\nu(2500\text{\AA}) = 2.5 \times 10^{47} \text{ erg s}^{-1}$ (Shemmer et al. 2014) deviates from the general trend by an amount which appears significant, despite the relatively large spread around the average relation. Allowing for a gravitational amplification would not change α_{ox} but, changing $L_\nu(2500\text{\AA})$, could make this object fully consistent with the general distribution, similarly to the case of 2XMM J091301.0+525929 which is a confirmed lensed QSO (see Vagnetti et al. 2010, and refs. therein). The second clue concerns the Baldwin (1977) effect. With respect to the average negative correlation between the CIV equivalent width (EW) and $\lambda L_\lambda(1350\text{\AA})$ (Bian et al. 2012), again PG 1247+267, with $\text{EW}=39.5 \text{ \AA}$ (Shen et al. 2011), is deviant and would be brought to full consistency by allowing for gravitational lensing. An amplification of about 10 would at the same time: i) account for both these effects; ii) bring the Eddington ratio to ~ 1 and iii) make this object less luminous than S5 0836+071 and consistent with the $\tau_l - L$ relation.

A candidate damped Ly α system (DLA) at $z=1.223$ in the spectrum of PG 1247+267 was analyzed by Pettini et al. (1999). Though Turnshek & Rao (2002) consider the column density too low to classify this absorption system as DLA, according to the conventional threshold $N_{HI} = 2 \times 10^{20} \text{ cm}^{-2}$, it could be associated with a foreground lensing galaxy. Of course this does not exclude that anisotropic (close to face-on) emission, possible intrinsic super-Eddington emission, and gravitational lensing occur at the same time. This suggests to further observe the spectral variability to perform velocity resolved RM, and also to investigate lensing evidences. Finally we remark that PG 1247+267 is the 5-th most luminous of $\sim 100,000$ QSOs in the Shen et al. (2011) catalog. Among the most luminous objects, the fraction of lensed QSOs could be high enough to bias the SE mass estimates and the studies of the evolution of both the mass function and the Eddington ratio distribution in cosmic time.

We acknowledge funding from PRIN/MIUR-2010 award 2010NHBSBE. This research is based on observations collected at Copernico telescope (Asiago, Italy) of the INAF - Osservatorio Astronomico di Padova, and at Cassini Telescope (Loiano, Italy) of the INAF - Osservatorio Astronomico di Bologna.

REFERENCES

Alexander, T. 1997, in *Astrophysics and Space Science Library*, Vol. 218, *Astronomical Time Series*, ed. D. Maoz, A. Sternberg, & E. M. Leibowitz, 163

- Assef, R. J., Denney, K. D., Kochanek, C. S., et al. 2011, *ApJ*, 742, 93
- Bachev, R., Marziani, P., Sulentic, J. W., et al. 2004, *ApJ*, 617, 171
- Baldwin, J. A. 1977, *ApJ*, 214, 679
- Bentz, M. C., Peterson, B. M., Netzer, H., Pogge, R. W., & Vestergaard, M. 2009, *ApJ*, 697, 160
- Bentz, M. C., Peterson, B. M., Pogge, R. W., Vestergaard, M., & Onken, C. A. 2006, *ApJ*, 644, 133
- Bentz, M. C., Denney, K. D., Grier, C. J., et al. 2013, *ApJ*, 767, 149
- Bessell, M. S. 1990, *PASP*, 102, 1181
- Bian, W.-H., Fang, L.-L., Huang, K.-L., & Wang, J.-M. 2012, *MNRAS*, 427, 2881
- Blandford, R. D., & McKee, C. F. 1982, *ApJ*, 255, 419
- Chelouche, D., Daniel, E., & Kaspi, S. 2012, *ApJ*, 750, L43
- Denney, K. D. 2012, *ApJ*, 759, 44
- Edelson, R. A., & Krolik, J. H. 1988, *ApJ*, 333, 646
- Ferrarese, L., & Merritt, D. 2000, *ApJ*, 539, L9
- Gaskell, C. M., & Peterson, B. M. 1987, *ApJS*, 65, 1
- Gaskell, C. M. 2009, *New Astronomy Reviews*, 53, 140
- Greene, J. E., Peng, C. Y., & Ludwig, R. R. 2010, *ApJ*, 709, 937
- Kaspi, S., Brandt, W. N., Maoz, D., et al. 2007, *ApJ*, 659, 997
- Kaspi, S., Maoz, D., Netzer, H., et al. 2005, *ApJ*, 629, 61
- Kaspi, S., Smith, P. S., Netzer, H., et al. 2000, *ApJ*, 533, 631
- Kelly, B. C., Bechtold, J., & Siemiginowska, A. 2009, *ApJ*, 698, 895
- Kozłowski, S., Kochanek, C. S., Udalski, A., et al. 2010, *ApJ*, 708, 927
- Krawczyk, C. M., Richards, G. T., Mehta, S. S., et al. 2013, *ApJS*, 206, 4
- MacLeod, C. L., Ivezić, Ž., Kochanek, C. S., et al. 2010, *ApJ*, 721, 1014
- Marconi, A., Risaliti, G., Gilli, R., et al. 2004, *MNRAS*, 351, 169
- Marziani, P., & Sulentic, J. W. 2012, *New Astronomy Reviews*, 56, 49
- McGill, K. L., Woo, J.-H., Treu, T., & Malkan, M. A. 2008, *ApJ*, 673, 703
- McIntosh, D. H., Rieke, M. J., Rix, H.-W., Foltz, C. B., & Weymann, R. J. 1999, *ApJ*, 514, 40
- McLure, R. J., & Jarvis, M. J. 2002, *MNRAS*, 337, 109
- Metzroth, K. G., Onken, C. A., & Peterson, B. M. 2006, *ApJ*, 647, 901
- Netzer, H. 2003, *ApJ*, 583, L5
- Netzer, H., Lira, P., Trakhtenbrot, B., Shemmer, O., & Cury, I. 2007, *ApJ*, 671, 1256
- Onken, C. A., Ferrarese, L., Merritt, D., et al. 2004, *ApJ*, 615, 645
- Onken, C. A., & Peterson, B. M. 2002, *ApJ*, 572, 746
- Pancoast, A., Brewer, B. J., Treu, T., et al. 2013, *arXiv.org*, 6475
- Perna, M., Trevese, D., Vagnetti, F., & Saturni, F. G. 2014, *Advances in Space Research*, 54, 1429
- Peterson, B. M. 1993, *PASP*, 105, 247
- Peterson, B. M., & Wandel, A. 1999, *ApJL*, 521, L95
- Peterson, B. M., Wanders, I., Bertram, R., et al. 1998, *ApJ*, 501, 82
- Peterson, B. M., Ferrarese, L., Gilbert, K. M., et al. 2004, *ApJ*, 613, 682
- Peterson, B. M., Bentz, M. C., Desroches, L.-B., et al. 2005, *ApJ*, 632, 799
- . 2006, *ApJ*, 641, 638
- Pettini, M., Ellison, S. L., Steidel, C. C., & Bowen, D. V. 1999, *ApJ*, 510, 576
- Pickles, A., & Depagne, É. 2010, *PASP*, 122, 1437
- Press, W. H., Rybicki, G. B., & Hewitt, J. N. 1992, *ApJ*, 385, 416
- Press, W. H., Teukolsky, S. A., Vetterling, W. T., & Flannery, B. P. 2007, *Numerical Recipes, The Art of Scientific Computing*, Third Edition (Cambridge University Press), 824
- Ramsey, L. W., Adams, M. T., Barnes, T. G., et al. 1998, in *Society of Photo-Optical Instrumentation Engineers (SPIE) Conference Series*, Vol. 3352, *Advanced Technology Optical/IR Telescopes VI*, ed. L. M. Stepp, 34–42
- Runnoe, J. C., Brotherton, M. S., DiPompeo, M. A., & Shang, Z. 2014, *MNRAS*, 438, 3263
- Runnoe, J. C., Brotherton, M. S., Shang, Z., & DiPompeo, M. A. 2013, *MNRAS*, 434, 848

- Rybicki, G. B., & Kleyana, J. T. 1994, in *Astronomical Society of the Pacific Conference Series*, Vol. 69, *Reverberation Mapping of the Broad-Line Region in Active Galactic Nuclei*, ed. P. M. Gondhalekar, K. Horne, & B. M. Peterson, 85
- Rybicki, G. B., & Press, W. H. 1992, *ApJ*, 398, 169
- Saturni, F. G., Trevese, D., Vagnetti, F., & Perna, M. 2014, *Advances in Space Research*, 54, 1434
- Shemmer, O., Brandt, W. N., Paolillo, M., et al. 2014, *ApJ*, 783, 116
- Shen, Y., & Kelly, B. C. 2012, *ApJ*, 746, 169
- Shen, Y., Richards, G. T., Strauss, M. A., et al. 2011, *ApJS*, 194, 45
- Sluse, D., Schmidt, R., Courbin, F., et al. 2011, *Astronomy and Astrophysics*, 528, 100
- Sulentic, J. W., Bachev, R., Marziani, P., Negrete, C. A., & Dultzin, D. 2007, *ApJ*, 666, 757
- Sulentic, J. W., Marziani, P., Zamanov, R., et al. 2002, *ApJ*, 566, L71
- Trevese, D., Paris, D., Stirpe, G. M., Vagnetti, F., & Zitelli, V. 2007, *A&A*, 470, 491
- Trevese, D., Saturni, F. G., Vagnetti, F., et al. 2013, *A&A*, 557, A91
- Turnshek, D. A., & Rao, S. M. 2002, *ApJ*, 572, L7
- Vagnetti, F., Turriziani, S., Trevese, D., & Antonucci, M. 2010, *A&A*, 519, A17
- Vestergaard, M. 2002, *ApJ*, 571, 733
- Vestergaard, M. 2004, *ApJ*, 601, 676
- Vestergaard, M., & Peterson, B. M. 2006, *ApJ*, 641, 689
- Wandel, A., Peterson, B. M., & Malkan, M. A. 1999, *ApJ*, 526, 579
- White, R. J., & Peterson, B. M. 1994, *PASP*, 106, 879
- Zu, Y., Kochanek, C. S., Kozłowski, S., & Peterson, B. M. 2013, *arXiv.org*, 6774
- Zu, Y., Kochanek, C. S., Kozłowski, S., & Udalski, A. 2013, *ApJ*, 765, 106
- Zu, Y., Kochanek, C. S., & Peterson, B. M. 2011, *ApJ*, 735, 80